Physica Scripta. Vol. T59 341–351, 1995

Plasmas With a Single Sign of Charge (An Overview)

Thomas M. O'Neil

Department of Physics, 0319, University of California at San Diego, La Jolla, California 92093-0319, U.S.A.

Received August 22, 1994; accepted January 31, 1995

Abstract

This paper presents a brief overview of recent theory and experiment for plasmas with a single sign of charge. In principle these plasmas can be confined forever in a state of thermal equilibrium that is guaranteed to be stable and quiescent. In practice confinement times of hours are routinely obtained. The plasmas can be cooled to the cryogenic temperature range where liquid and crystal-like states are predicted and observed. The plasmas provide experimental access to the parameter regime of strong magnetization where a many particle adiabatic invariant constrains the collisional dynamics. Also, the plasmas can be used to model the 2D vortex dynamics and turbulence of an ideal (incompressible and inviscid) fluid

1. Introduction

This paper discusses plasmas with a single sign of charge. Examples of such plasmas that have been realized in recent experiments are pure electron plasmas [1–7], pure ion plasmas of one or more species [8–10], and positron plasmas [11]. The requirement is that the plasmas be totally unneutralized, and in that sense the plasmas are a subset of the more general class of non-neutral plasmas [12].

Plasmas with a single sign of charge are typically confined in a Penning trap, and Fig. 1 shows a simple example of such a trap [1]. A conducting cylinder is divided axially into three sections with the central section held at ground potential and the two end sections held at positive potential (to confine positively charged particles). Also there is a uniform axial magnetic field. The plasma resides in the region of the central grounded section and is confined radially by the magnetic field and axially by the electric fields.

We will find that long-term confinement in a state of thermal equilibrium requires the trap to have cylindrical symmetry, but there are many variations consistent with this requirement. For example, the cylindrical electrodes may be replaced by hyperbolas of revolution; such traps have traditionally been used to confine small numbers of charged particles [13]. Also, the magnetic field need not be uniform, so long as it has the required cylindrical symmetry. As a specific example, let us consider the simple configuration shown in Fig. 1; this configuration has been used in most of the recent experiments.

Radial force balance requires that the plasma rotate about its axis. Because the plasma is non-neutral, the rotation produces an azimuthal current, and the radially inward $\boldsymbol{J} \times \boldsymbol{B}/c$ force balances all of the outward forces: the radial electric force, the radial pressure gradient, and the centrifugal force. Rotation through a magnetic field is in some sense like neutralization by a background charge. This is a useful way to think about these systems, and the idea will be made more precise as we proceed.

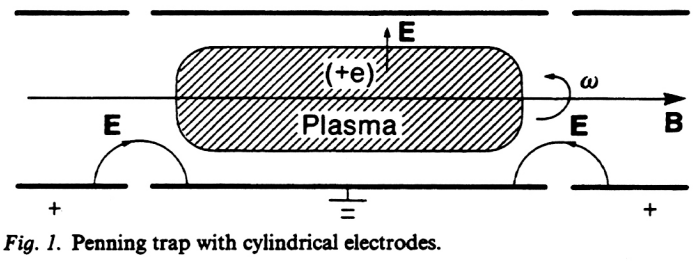

Fig. 1. Penning trap with cylindrical electrodes.

One of the first questions that you may want to ask is "Why do I insist on calling this collection of unneutralized charges a plasma?" The answer is that these systems exhibit much of the collective phenomena associated with ordinary neutral plasmas. For example, the measured dispersion relation for Langmuir waves in a pure electron plasma [14] is the same as it is for Langmuir waves in a neutral plasma (except for the Doppler shift associated with rotation of the electron plasma). To understand this result, simply recall that Langmuir waves occur at such a high frequency in a neutral plasma that the ions don't participate in the motion. Also, non-neutral plasmas exhibit Debye shielding [15]. To be precise, the Debye length ($\lambda_D = \sqrt{kT/4\pi ne^2}$) must be small compared to the dimensions of the plasmas for the collection of charges to qualify as a plasma. For a review of collective aspects of non-neutral plasmas emphasizing their similarity to neutral plasmas I refer you to Davidson's recent monograph on this subject [12].

Here, I take a different approach and emphasize some ways in which non-neutral plasmas (or more precisely, plasmas with a single sign of charge) differ from neutral plasmas. I want to identify and explore some unique research opportunities presented by these novel systems.

2. A Confinement theorem

One of the ways in which a plasma with a single sign of charge differs from a neutral plasma is that a plasma with a single sign of charge has superior confinement properties. In principle, such a plasma can be confined forever.

Referring again to Fig. 1, one can see that the axial confinement is guaranteed simply by turning the voltage on the end electrodes sufficiently high. It is the radial confinement (the magnetic confinement) that one must worry about. To understand this confinement, it is useful to introduce the total canonical angular momentum

$$P_\theta = \sum_{j=1}^{N} m v_{\theta j} r_j + \frac{e}{c} A_\theta(r_j) r_j, \tag{1}$$

where (z, r, θ) are cylindrical coordinates and the sum runs over all of the particles in the plasma. The quantity $(mv_{\theta j} r_j$ is the mechanical part of the angular momentum for the jth particle and the quantity $(e/c)A_\theta(r_j)r_j$ is the vector potential part. For a uniform axial magnetic field $A_\theta(r) = Br/2$; the

diamagnetic field is negligible for the low densities and velocities that we have in mind here. For a sufficiently large magnetic field, the vector potential contribution to the angular momentum is larger than the mechanical contribution, and eq. (1) reduces to

$$P_\theta \simeq \sum_{j=1}^{N} \frac{eB}{2c} r_j^2. \tag{2}$$

Since the plasma contains only a single sign of charge, the charge can be pulled out in front of the sum along with the other constants, and eq. (2) reduces to

$$P_\theta \simeq \frac{eB}{2c} \sum_{j=1}^{N} r_j^2. \tag{3}$$

To the extent that the confinement geometry has cylindrical symmetry, the N-particle Hamiltonian is invariant under rotation, and P_θ is a constant of the motion. Consequently, eq. (3) implies a constraint on the allowed radial positions of the particles; the mean square radius of the plasma is conserved.

This is a very powerful constraint, and it can be illustrated by a simple example. Fig 2 shows the end view of a plasma column that is initially shaped like a cylindrical shell of radius 1 cm [i.e., $r_j(t = 0) = 1\,\text{cm}$ for $j = 1, \ldots, N$]. The plasma resides in a long trap with the conducting wall at radius $r = 10\,\text{cm}$. Taking this situation as the initial condition, that will be the dynamical evolution of the plasma? It turns out that a hollow column is unstable to diocotron modes [3, 16]; so these modes grow to large amplitude, nonlinear effects come into play, and a turbulent-like evolution ensues. Interparticle collisions also effect the evolution, particularly the long time evolution. However, all of this complicated dynamics involves only internal interactions, so $P_\theta \propto \sum_j r_j^2$ is conserved. This means that only 1% of the particles can ever move from $r_j(0) = 1\,\text{cm}$ out to the wall at $r = 10\,\text{cm}$; the other 99% of the particles are confined forever.

This happy result is not realized for neutral plasmas. The constraint $\sum_j r_j^2 = \text{constant}$ is replaced by $\sum_j e_j r_j^2 = \text{constant}$, so an electron and an ion can move to the wall together and still preserve the sum. This is precisely what happens in electron-ion collisional transport as well as in many instabilities. One can see that it is much easier to confine a plasma with a single sign of charge than it is to confine a neutral plasma.

Of course, in a real experiment there are effects which break the cylindrical symmetry of the confinement geometry, so P_θ is not conserved exactly. For example, there are neutrals, and collisions of the plasma particles with these neutrals apply a torque on the plasma and allow the mean square plasma radius to expand [17, 18]. (Recall that the plasma has a net rotational motion relative to the lab frame and the neutrals.) Also, construction errors and field errors break the cylindrical symmetry and apply a torque on the plasma [18, 19, 10]. However, if one is careful to maintain a very good vacuum and to minimize construction and field errors, the net torque can be kept small and the confinement time long. Pure electron plasmas have been confined for hours with very little expansion observed [20].

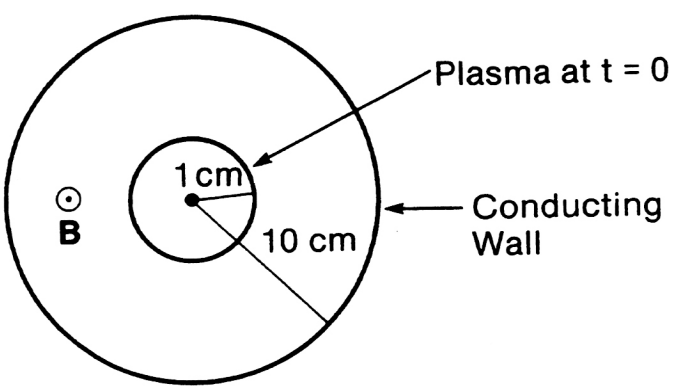

Fig. 2. End view of plasma column shaped like a cylindrical shell.

Finally, the argument leading to the angular momentum constraint was heuristic and various theoretical worries arise on closer inspection. For example, one might worry that the angular momentum radiated by the charges would lead to a non-negligible plasma expansion. Also, one might worry that the mechanical part of the angular momentum would grow to be comparable to the vector potential part as the charges move radially outward and gain kinetic energy; recall that the radial electric field does work on a charge as the charge moves outward.

To dispel such worries a confinement theorem was constructed using conservation of angular momentum and conservation of energy for the charge-field system [21]. The theorem applies to a long column in a region of space bounded by a perfectly conducting and perfectly absorbing cylindrical wall. Perfectly absorbing means that plasma particles cannot bounce off the wall and re-enter the plasma. The theorem assumes that A, $A^2(R\Omega_c/c) \ll 1$, where R is the radius of the conducting wall, $\Omega_c = eB/mc$ is the cyclotron frequency, and $A^2 = W_0/\sum_j m\Omega_c^2 r_j^2/2$. Here, W_0 is the initial kinetic plus electrostatic energy of the plasma. Typically, the kinetic energy is small compared to the electrostatic energy; so $A^2 \sim \omega_p^2/\Omega_c^2$, where ω_p is the plasma frequency. The theorem states that the sum $\sum_j r_j^2$ can change significantly only as a result of external torques (e.g., torques due to collisions with neutrals, field errors, etc.).

3. Boltzmann distribution

In practice the external torques can be made sufficiently weak that interactions between the plasma particles have time to bring the particles into thermal equilibrium with each other before there is significant plasma expansion [2, 8]. Consequently, we neglect the torques and study the thermal equilibrium states.

For a weakly correlated plasma in which the angular momentum and energy are both conserved, the Boltzmann distribution takes the form [22–24]

$$f = n_0 \left(\frac{m}{2\pi kT}\right)^{3/2} \exp\left[-\frac{1}{kT}(h + \omega p_\theta)\right], \tag{4}$$

where

$$h = \frac{mv^2}{2} + e\phi(r, z) \tag{5}$$

is the single particle Hamiltonian and

$$p_\theta = mv_\theta r + \frac{eB}{c}\frac{r^2}{2} \tag{6}$$

is the single particle canonical angular momentum. In eq. (5), the quantity $\phi(r, z)$ is the mean field (or Vlasov) electrical potential [25, 12]. The distribution is characterized by three parameters (n_0, T, ω), and these parameters are determined by the total number of particles, the total energy, and the total canonical angular momentum in the system (i.e., N, H, P_θ).

Substituting eqs (5) and (6) into eq. (4) and doing a small amount of algebra yields the distribution

$$f = n(r, z)\left(\frac{m}{2\pi k_B T}\right)^{3/2} \exp\left[-\frac{m}{2k_B T}(v + \omega r\hat{\theta})^2\right], \tag{7}$$

where

$$n(r, z) = n_0 \exp\left\{-\frac{1}{k_B T}[e\phi(r, z) + m\omega(\Omega_c - \omega)r^2/2]\right\}. \tag{8}$$

One can see that the velocity dependence is Maxwellian in a frame that rotates with frequency $-\omega$. As one expects, the thermal equilibrium distribution corresponds to a shear free flow; we call such a flow a rigid rotor. The density distribution is determined by three potentials: the electric potential $\phi(r, z)$, the centrifugal potential $-m\omega^2 r^2/2$, and the potential $m\omega\Omega_c r^2/2$. This latter potential is associated with the electric field induced by rotation through a magnetic field; it is this field that provides the radial confinement. To see that the distribution does in fact correspond to a confined plasma, note that $\phi(r, z)$ forces the distribution to be exponentially small at the ends of the column (assuming that the potential on the end electrodes is turned up sufficiently high) and that the potential $m\omega\Omega_c r^2/2$ forces the distribution to be exponentially small at large r (assuming that B is sufficiently large). Of course, the conducting wall is assumed to be outside the radius where the distribution becomes exponentially small.

Note that such thermal equilibrium distributions do not correspond to confinement for a neutral plasma. The sign of the charge enters $e\phi(r, t)$ and $m\omega\Omega_c r^2/2$, so confinement of electrons means non-confinement of ions. In fact, it is well known that a neutral plasma cannot be in thermal equilibrium and also be confined by static electric and magnetic fields; if it could, the controlled fusion problem would have been solved long ago. Because a confined neutral plasma is not in thermal equilibrium, there is always free energy to drive instabilities, and these instabilities have plagued controlled fusion research over the years. In contrast, a thermal equilibrium plasma with a single sign of charge is in a state of minimum free energy and is guaranteed to be stable. One must recall that this whole discussion is limited to time scales on which P_θ is well conserved.

In eq. (8), the electric potential is determined largely by the plasma charge density itself; so we must solve for the potential self-consistently [24]. In particular, we have to solve Poisson's equation,

$$\nabla^2\phi = 4\pi e n(r, z), \tag{9}$$

subject to the boundary conditions that specify the value of $\phi(r, z)$ on the conducting wall. Here, $n(r, z)$ is the density distribution given by eq. (8).

Assuming that the Debye length is small compared to the dimensions of the plasma, the self-consistent density turns out to be nearly constant out to some surface of revolution

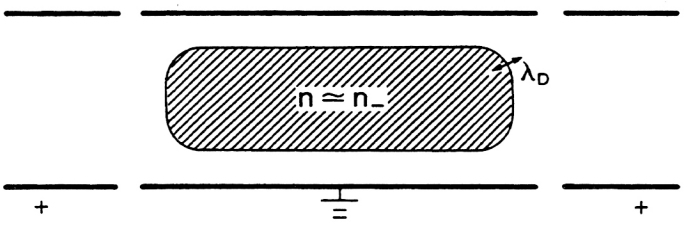

Fig. 3. Thermal equilibrium density distribution.

and then falls off on the scale of the Debye length (see Fig. 3) [24]. The fall off in density along the local normal to the surface of revolution is shown in Fig. 4, for the case where the Debye length is small compared to the local radius of curvature of the surface.

It is easy to understand this result in physical terms. First note that the second term in the bracket of eq. (8) is quadratic in r. Suppose that instead of being confined by a magnetic field, the plasma particles were confined by an imaginary cylinder of uniform negative charge. The potential energy of a positive charge e in the cylinder of negative charge would be quadratic in r; so the second term in the bracket of eq. (8) can be interpreted as such a potential energy. In other words, the thermal equilibrium density distribution for a magnetically confined plasma is the same as the thermal equilibrium density distribution for a plasma confined by a cylinder of neutralizing charge.

There is also charge on the positively biased end electrodes. This charge and the uniform cylinder of negative charge produce a potential well $\phi_0(r, z)$, and the plasma of positive charges resides in this well. Let us imagine building up the plasma step by step. When we introduce the plasma charges, they go to the bottom of the well and match their density to the density of imaginary negative charge. Gradually the well is filled up out to some surface of resolution where the supply of plasma is exhausted, and there the plasma density falls off on the scale of a Debye length. This is just the nature of the solution obtained by solving eqs (8) and (9) for the self-consistent potential and density [24].

The plasma density interior to the surface of revolution is very nearly equal to the density of the imaginary negative

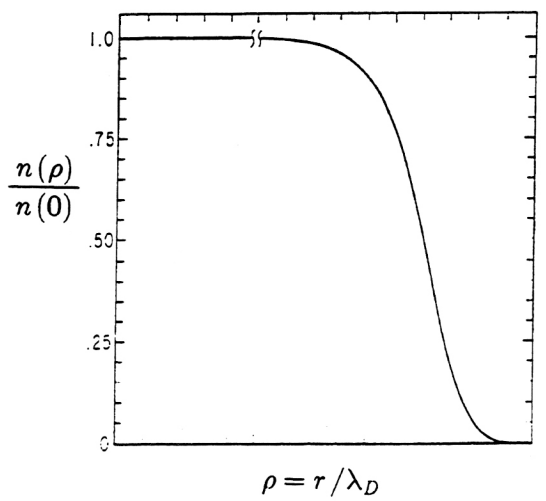

Fig. 4. Fall in density near plasma edge. The Debye length is assumed to be small compared to the local radius of curvature of the surface that defines the plasma edge (from Ref. [24]).

charge, and this density is given by

$$4\pi e^2 n_- = \nabla^2 m\omega(\Omega_c - \omega)r^2/2. \tag{10}$$

Evaluating the Laplacian and introducing the plasma frequency ($\omega_p^2 = 4\pi n e^2/m$) yields the useful result

$$\omega_p^2 = 2\omega(\Omega_c - \omega). \tag{11}$$

Equivalent to the statement that the plasma density is constant in the interior of the plasma is the statement that the sum of the two potentials in the bracket of eq. (8) is constant. This in turn implies that $E_z = \partial\phi/\partial z = 0$; the component of the electric field parallel to the magnetic field is Debye shielded out in the interior of the plasma, as one expects.

For given potentials on the end electrodes and a given value of $m\omega(\Omega_c - \omega)$, one can determine the shape of the potential well $\phi_0(r, z)$. Of course, the shape of this well is important in determining the shape of the plasma (the surface of revolution). For the simple case of a small plasma at the bottom of the well, the potential is approximately quadratic and can be written as

$$e\phi_0(r, z) \simeq C + \frac{m\omega_z^2}{2}(z^2 - r^2/2) + \frac{m\omega(\Omega_c - \omega)r^2}{2}, \tag{12}$$

where C and ω_z are constants. For this case, the plasma takes the shape of a spheroid (an ellipse of revolution) [8, 10, 26].

The reason for this is easy to understand. The bracket of eq. (8) is the sum of $e\phi_0$ and $e\phi_p$ where ϕ_p is the plasma space charge potential. This latter potential satisfies Poisson's equation and vanishes everywhere on the conducting boundary. Inside the plasma, the bracket is constant, so when ϕ_0 is quadratic, ϕ_p must be quadratic. It is well known that a uniformly charged spheroid in free space produces a quadratic potential inside the spheroid. If the plasma is small compared to the distance to the conducting boundary, the free space solution is a good approximation. The aspect ratio of the ellipse is related to the coefficients in ϕ_0 through [10]

$$\frac{\omega_z^2}{2\omega(\Omega_c - \omega)} = g(Z_p/R_p), \tag{13}$$

where

$$g(x) = Q_1^{(0)}[x/(1 - x^2)^{1/2}]/(x^2 - 1). \tag{14}$$

Here, Z_p/R_p is the aspect ratio and $Q_1^{(0)}$ is the associated Legendre function of the second kind.

For given values of the density and magnetic field strength (or, equivalently, given values of ω_p^2 and Ω_c), eq. (11) determines two possible rotation frequencies [27]

$$\omega_\pm = \frac{\Omega_c \pm \sqrt{\Omega_c^2 - 2\omega_p^2}}{2}. \tag{15}$$

The frequencies are real only if $2\omega_p^2/\Omega_c^2 \leq 1$; this inequality sets the maximum density that can be confined for a given magnetic field strength and is referred to as the Brillouin limit [27]. In Fig. 5, $\omega_\pm/\Omega_c$ are plotted as a function of $2\omega_p^2/\Omega_c^2$; the solution ω_+ lies on the upper half of the parabola and the solution ω_- on the lower half. For a long column, equilibria exist for the full range of frequencies $0 < \omega < \Omega_c$. For a small spheroidal plasma in a quadratic trap

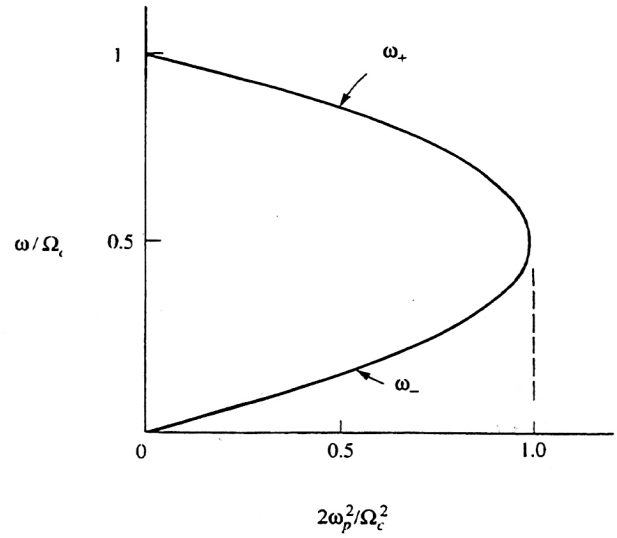

Fig. 5. Plasma rotation frequency as a function of plasma density and magnetic field strength.

potential, equilibria exist only for the frequency range $\omega_m < \omega < \Omega_c - \omega_m$, where $\omega_m = \Omega_c/2 - (\Omega_c^2/4 - \omega_z^2/z)^{1/2}$ is the single particle magnetron frequency, that is, the drift frequency of a single particle in the trap potential [10]. One can see from eqs (11), (13) and (14) that Z_p/R_p approaches zero as ω approaches ω_m or $\Omega_c - \omega_m$.

Note that the existence of the two solutions does not contradict our expectations that (N, H, P_θ) uniquely determine a thermal equilibrium state. Consider two solutions with the same value for $\omega_p^2 = 2\omega(\Omega_c - \omega)$, for T, and for the total number of particles N, but with different rotation frequencies ω_+ and ω_- as given by eq. (15). The two solutions have the same density distribution but different velocity distributions. Consequently, the values of H and of P_θ are different for the two solutions. In fact,

$$P_\theta = m(\Omega_c/2 - \omega)\int d^3r n(r, z)r^2 \tag{16}$$

differs for the two solutions by a minus sign, since $(\Omega_c/2 - \omega_+) = -(\Omega_c/2 - \omega_-)$. In general, P_θ is positive on the lower half of the parabola where $\omega < \Omega_c/2$, is negative on the upper half where $\omega > \Omega_c/2$, and vanishes at the Brillouin limit where $\omega = \Omega_c/2$.

To obtain further insight into the relation between the two solutions, we write the equation of motion for a particle in the rotating frame

$$m\frac{d\boldsymbol{v}}{dt} = m(\Omega_c - 2\omega)\boldsymbol{v} \times \hat{z} - \nabla[e\phi + m\omega(\Omega_c - \omega)r^2/2]. \tag{17}$$

The effective cyclotron frequency is called the vortex frequency $\Omega_v = \Omega_c - 2\omega$ [27]. Physically, the modification is due to the coriolis force. For the two solutions $\omega = \omega_\pm$, the last term on the r.h.s. of eq. (17) is the same, but the vortex frequencies differ by a minus sign [i.e., $(\Omega_c - 2\omega_-) = -(\Omega_c - 2\omega_+)$]. Thus, the equations of motion differ only in that the direction of the magnetic field is effectively reversed.

Interestingly, at the Brillouin limit ($\omega = \Omega_c/2$), the effective magnetic field vanishes (i.e., $\Omega_v = \Omega_c - 2\omega = 0$). Also, for small Debye length, the bracket on the r.h.s. of eq. (17) is constant inside the plasma. Thus, in the rotating frame, the particles follow straight line orbits within the plasma, reflec-

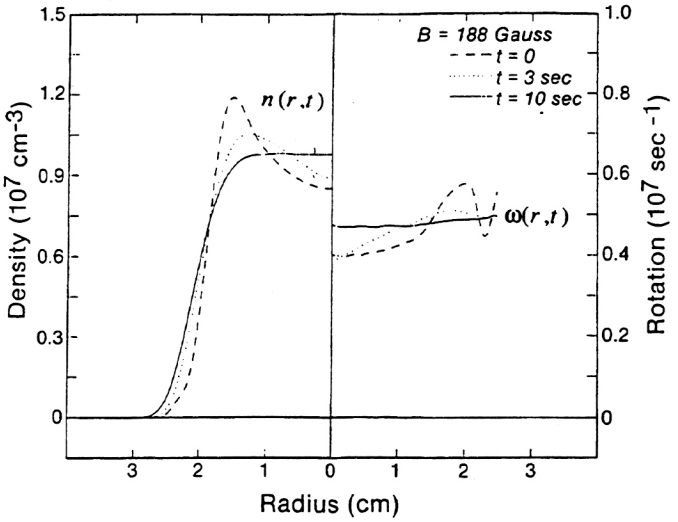

Fig. 6. Evolution to thermal equilibrium of a pure electron plasma column. The density and rotation frequency are shown as a function of radius for three times (from Ref. [2]).

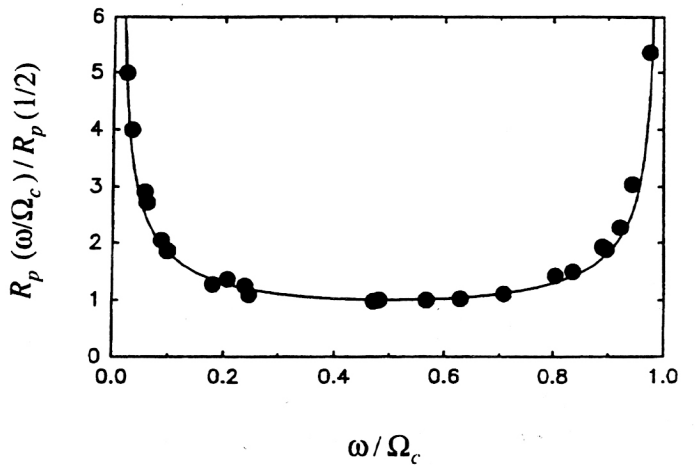

Fig. 9. Radius of a plasma of 2000 Be^+ ions as a function of the plasma rotation frequency. The radius is scaled to the radius at the Brillouin limit and the frequency to the cyclotron frequency. The solid curve is the theoretical prediction with no adjustable parameters (from Ref. [10]).

ting off of the Debye sheath at the edge. At the Brillouin limit, the dynamics of a Penning trap plasma is the same as that of an RF (Paul) trap, except for the RF micromotion of particles in the Paul trap.

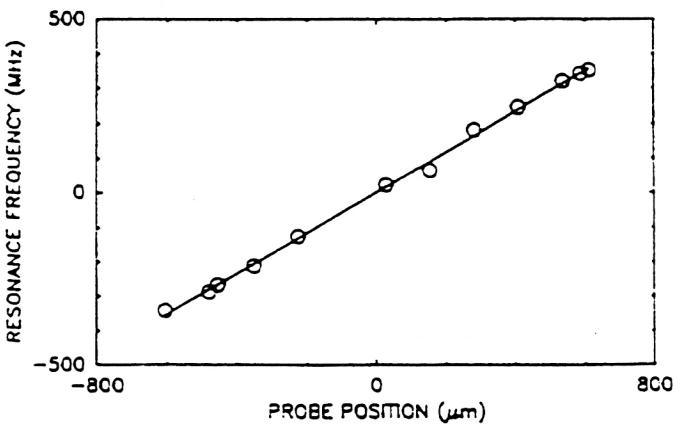

Fig. 7. Doppler shifted resonance frequency *vs.* the displacement of the laser beam from the plasma axis of rotation for a 30000 $^9Be^+$ ion plasma (from Ref. [8]).

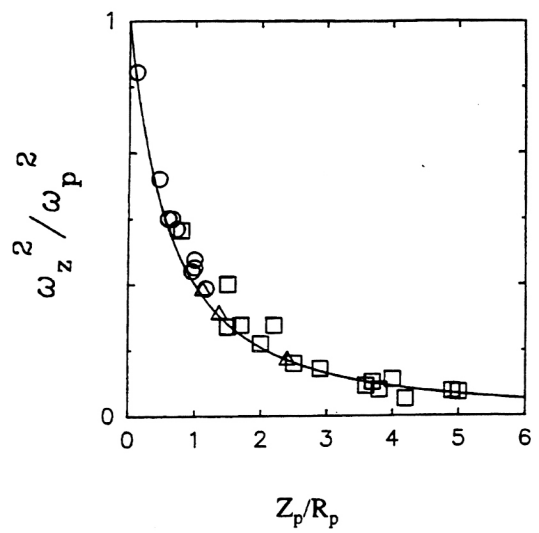

Fig. 8. Experimental check of eq. (13). Data were obtained for $^9Be^+$ plasmas with 2000 to 40000 Be^+ ions and for two different traps (from Ref. [8]).

Much of this theory has been verified experimentally. A signature of thermal equilibrium is that the rotational flow is shear free. Of course, for an arbitrary initial state, the local rotation frequency $\omega(r)$ is not uniform in r. The shears in the flow give rise to azimuthal viscous forces (due microscopically to collisions) that drive the plasma (through radial drifts) to a state of rigid rotation. Figure 6 shows the experimentally observed evolution of a pure electron plasma column to a thermal equilibrium state [2]. On the left the density profile $n(r, t)$ is plotted for the times $t = 0$, 3, 10 sec, and on the right the local rotation frequency $\omega(r, t)$ is plotted for the same three times. By $t = 10$ sec, the density profile has evolved to the expected thermal equilibrium form, and the rotation frequency has become nearly uniform in r.

Thermal equilibrium states also have been observed for pure ion plasmas [8]. A laser beam was passed through the plasma in a direction perpendicular to the axis of rotation and displaced a distance d from the axis. The doppler shift ν of the laser frequency relative to a resonance of the $^9Be^+$ ions that constituted the plasma was then measured for several values of d. Figure 7 shows that $\nu(d)$ was nearly linear, which is the expectation for shear free rigid rotation. For the case of a small ion plasma in a quadratic well, the plasma shape was observed to have the expected spheroidal shape [8]. Figure 8 shows the results of an experimental check of eq. (13), which relates the aspect ratio Z_p/R_p to the frequency ratio $\omega_z^2/2\omega(\Omega_c - \omega) = \omega_z^2/\omega_p^2$.

By using lasers to cool and exert a torque on the plasma (i.e., to vary H and P_θ), the rotational state of the plasma was continuously varied over the parabola in Fig. 5 [10]. Figure 9 shows a comparison of theory and experiment for the ratio $R_p(\omega/\Omega_c)/R_p(1/2)$ *vs*, ω/Ω_c. Here, $R_p(1/2)$ is the radius at the Brillouin limit ($\omega/\Omega_c = 1/2$). As expected, the ratio is even about $\omega/\Omega_c = 1/2$. Also, the agreement between theory and experiment is good over the whole range.

4. Strong correlation

Another advantage of plasmas with a single sign of charge is that they can be cooled to the cryogenic temperature range without the occurrence of recombination [28]. When kT

drops below e^2/a, where a is the distance between neighboring charges, the physics of strong correlation comes into effect. Since the characteristic mean-field potential is large (i.e., $e\phi \gg kT$, e^2/a), the correlations cannot change the gross plasma shape that was discussed in the previous section. Rather, order is established within that shape.

A measure of correlation strength is the coupling parameter $\Gamma \equiv e^2/akT$, where to be precise a is the Wigner-Seitz radius ($4\pi a^3 n/3 \equiv 1$) [29]. Of course, weak correlation occurs in the limit $\Gamma \ll 1$. Theoretical studies [29, 30] of a strongly correlated and infinite homogeneous one component plasma (OCP), that is, a system of point changes in a uniform neutralizing background charge, predict that the system begins to exhibit the local order characteristic of a liquid for $\Gamma \simeq 2$ and that there is a phase transition to a b.c.c. crystal for $\Gamma \simeq 172$.

Experiments with pure ion plasmas in a Penning trap [9, 10] have achieved Γ values in excess of a hundred, but the experiments involved a relatively small number of particles ($N \sim 10^2$ to 10^4), so the theoretical studies of an infinite homogeneous OCP cannot be trusted. On the other hand, these small plasmas are ideally suited for numerical simulation with a realistic (or nearly realistic) number of particles, and several authors have carried out such simulations [31–35].

Dubin and I carried out molecular dynamics simulations and Monte Carlo calculations with the trap fields and boundary conditions chosen to model the experiments [31]. In the molecular dynamics simulation, the equations of motion for N interacting charges in a Penning trap are integrated forward in time until the charges come into thermal equilibrium with each other. Average quantities such as the local density are determined as long time averages

$$n(x) = \frac{1}{T}\int_0^T dt \sum_{j=1}^{N} \delta[x - x_j(t)]. \tag{18}$$

According to the ergodic hypothesis, such a time average is equal to a phase space average weighted by a distribution for a microcanonical ensemble [36]

$$\rho_{\text{m.c.}} = C\delta[H - H(0)]\delta[P_\theta - P_\theta(0)], \tag{19}$$

where C is a normalization factor, H is the N-particle Hamiltonian, P_θ is the total canonical angular momentum, and $H(0)$ and $P_\theta(0)$ are the initial values of these quantities. This is the appropriate thermal distribution for an isolated system with H and P_θ conserved.

In contrast, the Monte Carlo calculation is a statistical game of chance based on the distribution for a canonical ensemble [23]

$$\rho_c = C' \exp\left[-\frac{1}{kT}(H - \omega P_\theta)\right], \tag{20}$$

where C' is a normalization factor. One considers a sequence of random steps for the N-particle phase point and conditions the acceptance or rejection of a given step by the change in the probability of the N-particle state, that is, the change in the value of ρ_c [37]. Averages are taken along the sequence of phase points generated in this way, and for a sufficiently long sequence, the average approaches the phase space average weighted by ρ_c.

This distribution represents a system with fixed values of the temperature T and rotation frequency ω, rather than fixed values of H and P_θ. The distribution is appropriate for a plasma in thermal contact with a heat and angular momentum reservoir. For example, Fig. 10 shows a trapped plasma in thermal contact with an infinitely long plasma column (the reservoir) characterized by temperature T and rotation frequency ω. Thermal fluctuations in the fields produce energy and angular momentum transfer back and forth between the plasma and the reservoir.

For a sufficiently large plasma, the fluctuations in plasma energy and angular momentum are small compared to the mean values of these quantities, so one expects the fluctuations to have negligible influence on the plasma structure. We find that the molecular dynamics simulation and the Monte Carlo calculation yield the same answer for average quantities such as the local density, provided that $N \gtrsim 100$, and we limit our consideration to such plasmas. In other words, we consider plasmas that are large in the sense that the micro-canonical and the canonical ensembles give the same answer but are small in the sense that boundedness affects the structure.

We can gain some useful insights from the canonical ensemble. Distribution (20) is of the same form as the Boltzmann distribution [eq. (4)], and one can carry out the same algebra as was carried out in passing from eq. (4) to eqs (7) and (8). One then concludes that the canonical ensemble for the magnetically confined plasma differs only by rotation from the canonical ensemble for a plasma confined by a cylinder of uniform neutralizing charge. In other words, the magnetically confined plasma has the same thermal equilibrium structure as a bounded OCP. As discussed in the last section, this OCP resides in a potential well $\phi_0(r, z)$ that is produced by the cylinder of uniform neutralizing charge and the end electrodes.

Another relationship that follows from the canonical ensemble concerns the guiding center dynamics that we employ in the molecular dynamics simulation [31]. In the experiments, the cyclotron radius typically is much smaller than the distance between particles, or equivalently, the cyclotron period is much shorter than an iteraction time. Under these circumstances it is useful to average out the high frequency cyclotron dynamics before turning to the computer. This is accomplished by using the guiding center equations of motion rather than the exact equations of motion. Although the guiding center equations are only approximate, the thermal equilibrium structure obtained with them is not. By substituting the guiding center Hamiltonian and guiding center angular momentum into distribution (20), one finds that the guiding center system has the same thermal equilibrium structure as the exact system, except for a slightly shifted magnetic field strength.

What follows are numerical results for the case of a small plasma at the bottom of the effective potential well (the experimental situation). The well in the region of the plasma is nearly quadratic as given in eq. (12). For convenience in

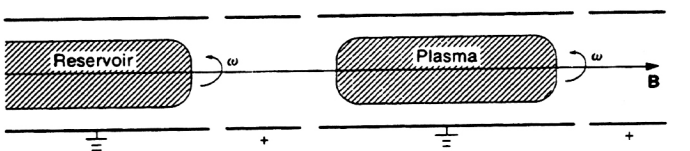

Fig. 10. Plasma in thermal contact with a heat and angular momentum reservoir.

displaying results, we choose conditions so that the well (and plasma) have spherical symmetry. The fact that the plasma radius is small compared to the radius of the conducting cylinder also implies that the force due to an image charge is small, so we take the interaction potential to be simply $e^2/|x_i - x_j|$.

Figure 11 shows the results of a Monte Carlo calculation for Γ values ranging from 1 to 10; the average density $n = n(r)$ is plotted as a function of the radius r for r values near the plasma edge. The potential well and plasma have spherical symmetry. For $\Gamma = 1$, the density falls smoothly to zero, as it does for weak correlation (see Fig. 3); but for higher values of Γ, oscillations are present near the plasma edge. These oscillations are evidence of local order; the damping length for the oscillations is a measure of the correlation length. One may think of the density maxima as embryonic lattice planes, or more precisely, spherical lattice shells.

Figure 12 shows the result of a molecular dynamics calculation for $\Gamma = 140$ and $N = 100$, again for spherical symmetry. The density is essentially zero between the spherical shells, and if you tag an individual particle on one of these shells you find that the particle is localized to the shell but not localized on the shell. For this value of Γ the particles still diffuse over the surface of the shell. The system behaves like a crystal in the radial direction, but like a liquid along the surface of a shell. Figure 13 shows density contours for a spherical plasma with $\Gamma = 190$ and $N = 256$.

For substantially higher values of Γ, the particle diffusion along the surface of a shell also goes to zero, and an imperfect 2D hexagonal crystal is formed on the shell. Figure 14 shows the outer half shell for a $N = 256$ spherical plasma with $\Gamma = 380$. The ions are arranged in an imperfect 2D hexagonal crystal and execute small amplitude thermal motion about their equilibrium positions.

The shell structure has been observed experimentally. Figure 15 shows an image of 11 shells for a plasma of 15 000 Be^+ ions [9]. Three laser beams were passed through the plasma exciting the Be^+ ions, and the ion fluorescence was then focussed to form the image.

New experiments [see paper by John Bollinger in these proceedings] with substantially larger plasmas ($N - 10^6$) are now being carried out, and it is interesting to ask how large the plasma must be to realize the bcc lattice structure

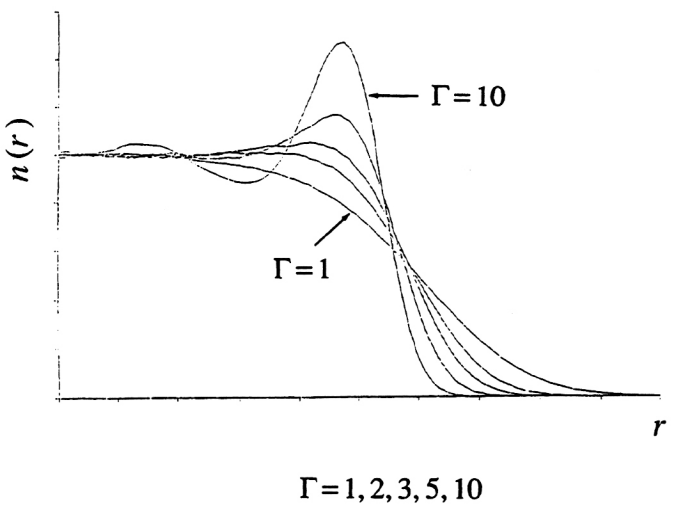

Fig. 11. Results of a Monte Carlo calculation for $\Gamma = 1, \ldots, 10$; the average density $n(r)$ is plotted for r values near the plasma edge.

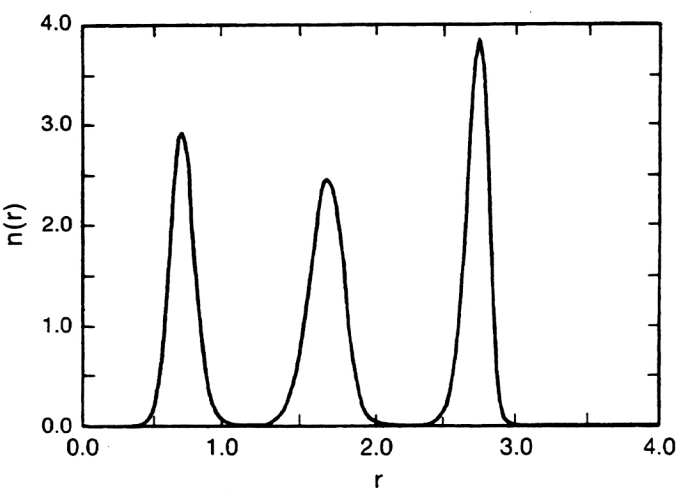

Fig. 12. Results of a molecular dynamics simulation for $\Gamma = 140$ and $N = 100$ with a spherical symmetry; the average density $n(r)$ is plotted as a function of r.

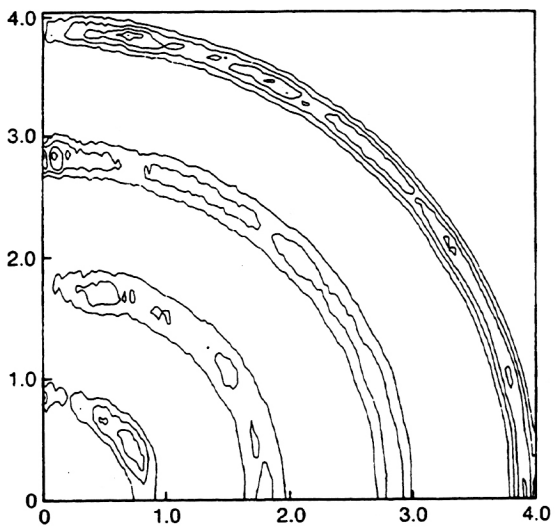

Fig. 13. Density contours for a spherically symmetric plasma obtained from molecular dynamics simulation for $\Gamma = 190$ and $N = 256$.

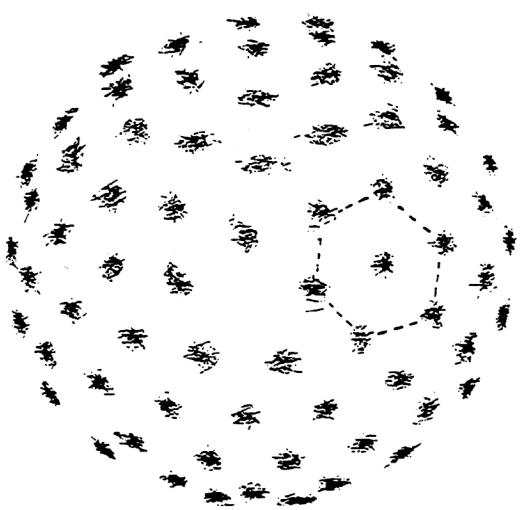

Fig. 14. Results of a molecular dynamics simulation for $\Gamma = 380$ and $N = 256$ with spherical symmetry. Particles in the outer shell are shown executing thermal motion about their equilibrium positions.

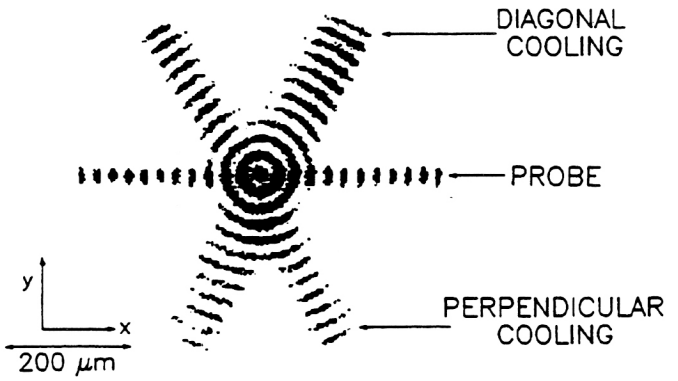

Fig. 15. Image of shell structure for a plasma of 15000 Be^+ ions (from Ref. [9]).

predicted for an infinite homogeneous OCP. Dubin has predicted that the plasma must be quite large (60 lattice planes) [38]. The reason is that the bulk binding energies for an fcc and a bcc lattice are nearly the same, so a relatively small surface contribution to the free energy can mask the difference. John Schiffer [39] has recently carried out a very ambitious molecular dynamics simulation involving $N = 20000$ charges, and shell structure was observed (see Fig. 16). In this simulation, the plasma was carefully cooled (annealed) to very low temperature, corresponding to values of Γ in excess of a thousand.

In summary, it is fair to say that the small, cold, thermal equilibrium plasmas in a quadratic trap potential are some of the best understood plasmas. A simple analytic theory predicts the gross plasma shape (spheroidal) and its dependence on trap parameters, and the predictions are in good agreement with experiment. Within the context of fluid theory, an analytic description has been obtained for all of the modes of oscillation about the equilibrium [40, 41], and the predicted frequencies (for the low order modes that have been checked thus far) are in good agreement with experiment (see paper by John Bollinger in these proceedings) [42, 43, 10]. Also, theory and experiment are converging to provide an understanding of the microscopic order within the spheroidal shape.

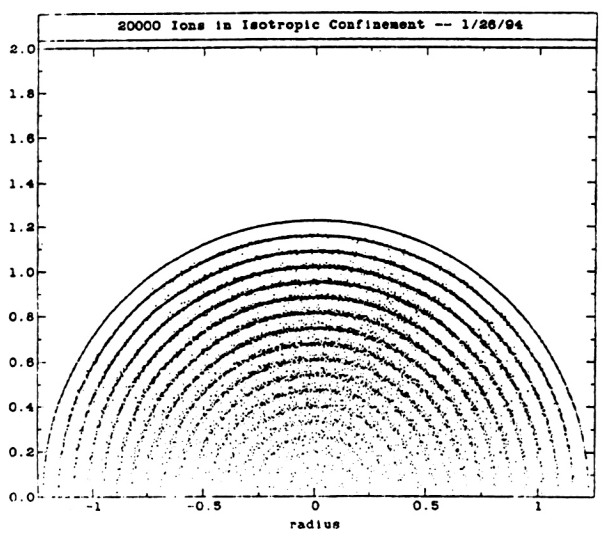

Fig. 16. Results of a molecular dynamics simulation for a $N = 20000$ spherical plasma with Γ in excess of a thousand (personal communication from J. Schiffer).

5. Strong magnetization

Cryogenic electron plasmas provide experimental access to the novel parameter regime of strong magnetization. We say that a plasma is strongly magnetized when the cyclotron frequency is the largest of the dynamical frequencies [44]. For a weakly correlated plasma ($\Gamma \ll 1$), the largest of the remaining frequencies is $\bar{v}/b$, where $\bar{v} = \sqrt{kT/m}$ is the thermal velocity and $b = e^2/kT$ is the classical distance of closest approach. Thus, strong magnetization requires that

$$\Omega_c \gg \bar{v}/b. \tag{21}$$

This inequality is most easily satisfied for electrons, and for this case it can be written as

$$10^{-7}B\ [\text{Gauss}] \gg (kT)^{3/2}\ [\text{eV}]. \tag{22}$$

One can see that strong magnetization requires low temperature as well as large magnetic field. Even for a magnetic field strength as large as 100 kG, the required temperature is such that a neutral plasma would recombine. Of course, the pure electron plasma cannot recombine, and as the temperature drops into the cryogenic range the plasma becomes strongly magnetized.

In this parameter regime the total action associated with the cyclotron dynamics,

$$J = \sum_{j=1}^{N} \frac{mv_{\perp j}^2}{2\Omega_c}, \tag{23}$$

is a many electron adiabatic invariant that constrains the collisional dynamics [44]. Here, $v_{\perp j}$ is the velocity perpendicular to the magnetic field. One may think of the cyclotron variables as high frequency oscillators and the remaining variables (the guiding center variables) as slowly varying parameters that modulate the high frequency oscillators. During a collision, the high frequency oscillators can exchange quanta (action) with each other but not with the low frequency variables, that is, the total cyclotron action is conserved, or more precisely, is an adiabatic invariant.

We are used to thinking about adiabatic invariants associated with a single particle. For example, for a particle in a slowly varying field, the magnetic moment $mv_\perp^2/2B$ (or equivalently, cyclotron action) is an adiabatic invariant. In contrast, we are discussing here a many particle invariant. One might think that the sum in eq. (23) is conserved simply because each of the terms is separately conserved, but that is not the case. During a collision between electron 1 and electron 2, the cyclotron motion of electron 2 introduces a high frequency component to the interaction field felt by electron 1, and this breaks the adiabatic invariant of electron 1. Likewise the invariant of electron 2 is broken by the high frequency field from electron 1. However, the sum of the two invariants is conserved.

For the case of a uniform magnetic field, the quantity Ω_c^{-1} may be factored out of the sum in eq. (23), so the total perpendicular kinetic energy is an adiabatic invariant. Because of this invariant, the collisional relaxation of the electron velocity distribution takes place in two stages. On the time scale of a few collisions, the adiabatic invariant is well conserved, so the velocity distribution becomes Maxwellian in the parallel direction and in the perpendicular direction separately with $T_\parallel$ not necesarily equal to $T_\perp$. However, the evolution does not stop at this stage, since an

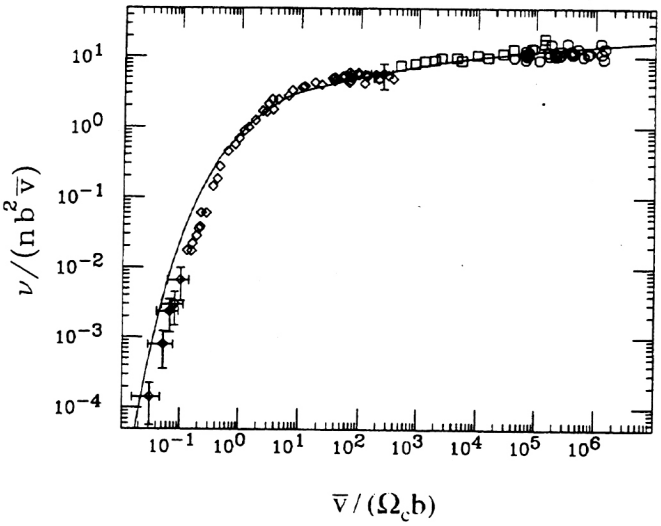

Fig. 17. Comparison of theory and experiment for the collisional equipartition rate (from Ref. [44]).

adiabatic invariant is not an exact constant of the motion. During each collision there is an exponentially small breaking of the adiabatic invariant, that is, an exponentially small exchange of parallel and perpendicular energy, and these act cumulatively to allow $T_\parallel$ and $T_\perp$ to relax to a common value.

Figure 17 shows a comparison of the theoretically predicted equipartion rate to the measured rate [44, 45]. Here, the rate ν is defined through the equation $dT_\perp/dt = \nu(T_\parallel - T_\perp)$. The ordinate in Fig. 17 is the scaled rate $\nu/(n\bar{v}b^2)$, where the combination $(n\bar{v}b^2)$ is very nearly the collision frequency for an unmagnetized plasma. According to theory, the scaled rate depends on temperature and magnetic field strength only through the combination $\bar{v}/(\Omega_c b)$. This quantity is the abscissa in the figure. One can see that theory and experiment are in good agreement over nearly eight decades in $\bar{v}/(\Omega_c b)$, and that the rate drops dramatically in the strongly magnetized regime [i.e., for $\bar{v}/(\Omega_c b) \ll 1$].

The theory has now been extended to the case of a strongly magnetized crystal [46]. In this case, the cyclotron phonons ($\omega \sim \Omega_c$) are of much higher frequency than the plasma phonons ($\omega \sim \omega_p$), and the total action associated with the cyclotron phonons is an adiabatic invariant. The rate of equilibration between $T_\parallel$ and $T_\perp$ is calculated to be $\nu \sim \omega_p \exp[-(\Omega_c/\omega_p)\ln(\Gamma\omega_p/\Omega_c)]$. The calculation assumes that $\Omega_c/\omega_p \gg 1$ and $\Gamma\omega_p/\Omega_c \gg 1$.

6. Turbulence and vortex dynamics

A pure electron plasma in a cylindrically symmetrical Penning trap is an ideal system for turbulence studies because the confinement theorem guarantees that the plasma remains confined in spite of the turbulence. The plasma evolution can be followed from an initial instability through the nonlinear stages of vortex formation and merger to decay of the turbulence. Also, by a happy coincidence, the low frequency $\boldsymbol{E} \times \boldsymbol{B}$ drift flow of the plasma models the 2D dynamics of an ideal (incompressible and inviscid) fluid [3].

When the plasma column is long and the cyclotron frequency and axial bounce frequency for a typical electron are large, the cross magnetic field flow of the plasma can be described by the 2D drift-Poisson equations

$$\boldsymbol{v} = \frac{c}{B}\hat{z} \times \nabla\phi$$

$$\frac{\partial n}{\partial t} + \boldsymbol{v} \cdot \nabla n = 0$$

$$\nabla^2\phi = 4\pi e n, \tag{24}$$

where $n = n(r, \theta, t)$ and $\phi = \phi(r, \theta, t)$. These equations are isomorphic to the equations that govern the 2D dynamics of an ideal fluid, with $(c/B)\phi$ corresponding to the stream function and $(4\pi ec/B)n$ to the vorticity [3].

There are several experimental advantages of studying the flow with a pure electron plasma, rather than with, say, water. The vorticity (electron density) can be imaged directly by dumping the electrons out along the magnetic field lines to a phosphorous screen (imaged by a CCD camera). Also, the pure electron plasma has very low viscosity, is constrained by the magnetic field and rapid bounce motion to be highly 2D, and is not complicated by boundary layers at the ends and walls.

Figure 18 shows a sequence of images in which two vortices (electron columns) undergo merger [47]. To obtain the time sequence of images, one relies on shot to shot reproducibility. The apparatus is operated repeatedly in an inject-hold-dump sequence always starting from the same initial condition but allowing successively longer hold times. In this way, one can make a "movie" of the dynamical evolution.

The time for merger is a sensitive function of the initial separation of the vortices. Figure 19 shows the merger time

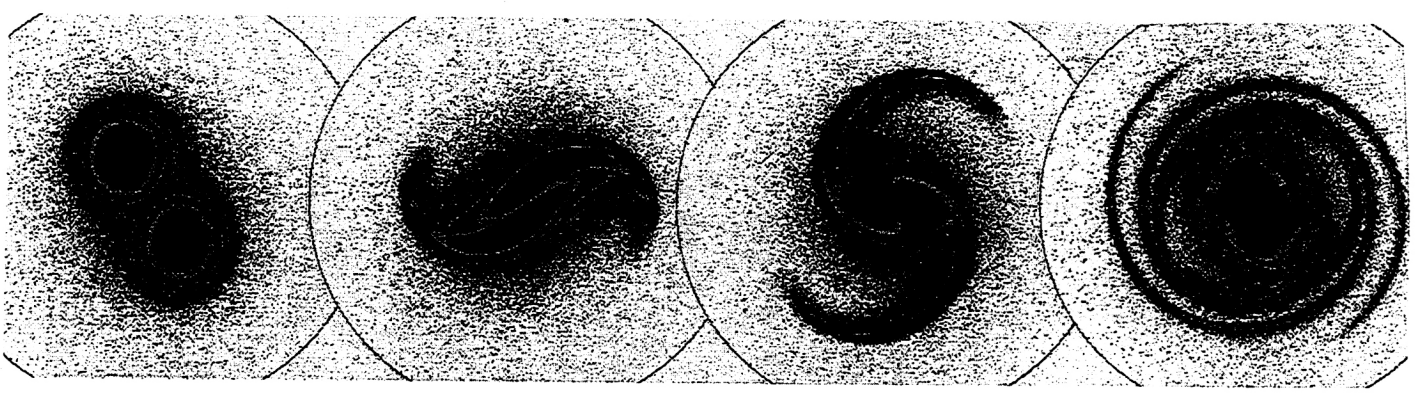

Fig. 18. Two vortices (electron columns) undergo merger. The pictures were obtained by dumping the electrons out along the magnetic field lines to a phosphorus screen imaged by a CCD camera (from Ref. [47]).

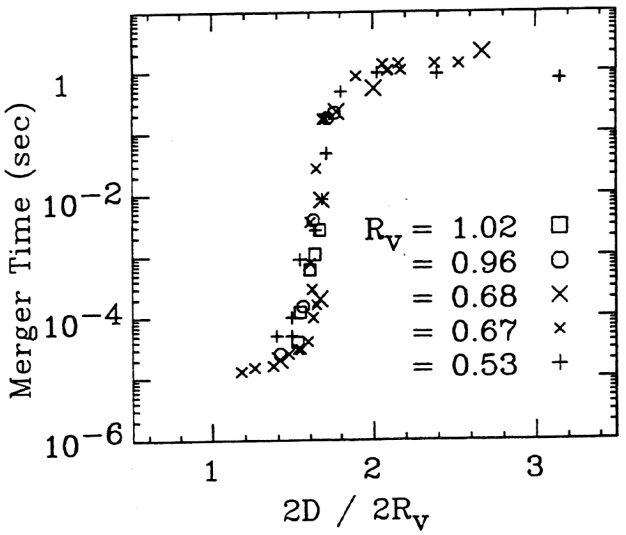

Fig. 19. Time for merger of two vortices *vs.* the ratio $2D/2R_v$, where $2D$ is the initial separation and $2R_v$ is the initial diameter (from Ref. [47]).

as a function of $2D/2R_v$, where $2D$ is the initial separation and $2R_v$ is the initial diameter [47]. The time for merger increases by 10^4 as D/R_v passes from 1.5 to 1.8. Figure 18 shows a case of rapid merger where $D/R_v = 1.48$. These results are in good agreement with analytic theory and numerical computation for 2D ideal fluids [48–50].

Figure 20 shows a time sequence of images that start from a highly unstable initial state [51]. The first image shows a plasma that already is highly filamented and has many small vortices. During the turbulent evolution, the small vortices merges to form larger vortices. Ultimately, the turbulence decays leaving a single, cylindrically symmetrical, stable vortex (plasma column). For other initial conditions, some of the vortices do not merge, but rather are annealed into a crystal structure. An interesting challenge to theory is to predict the final meta-equilibrium that results from the 2D-turbulence. For a wide class of initially unstable plasmas (hollow columns) the principle of minimum enstrophy provides an accurate prediction of the meta-equilibrium state [52]. However, it is clear that this principle must fail in some cases, as, for example, when the evolution leads to a crystal structure of vortices. This is a rich and interesting area of research and much work remains to be done.

Acknowledgements

This work was supported by U.S. Office of Naval Research Grant N00014-89-J-1714, National Science Foundation Grant No. PHY91-20240, and Department of Energy Grant No. DE-FG03-85ER53199.

References

1. de Grassie, J. S. and Malmberg, J. H., Phys. Fluids **23**, 63 (1980).
2. Driscoll, C. F., Malmberg, J. H. and Fine, K. S., Phys. Rev. Lett. **60**, 1290 (1988).
3. Driscoll, C. F. and Fine, K. S., Phys. Fluids **B2**, 1359 (1990).
4. Tan, J. and Gabrielse, G., Phys. Rev. **A48**, 3105 (1993).
5. Gould, R. W. and LaPointe, M. A., Phys. Rev. Lett. **67**, 3685 (1991).
6. Hart, G. W., Phys. Fluids **B3**, 2987 (1991).
7. Chu, R., Wurtele, J. S., Notte, J., Peurrung, A. J. and Fajans, J., Phys. Fluids **B5**, 2378 (1993).
8. Brewer, L. R. *et al.*, Phys. Rev. **A38**, 859 (1988).
9. Gilbert, S. L., Bollinger, J. J. and Wineland, D. J., Phys. Rev. Lett. **60**, 2022 (1988); Bollinger, J. J. and Wineland, D. J., Sci. American (January 1990), p. 124.
10. Bollinger, J. J., Wineland, D. J. and Dubin, D. H. E., Phys. Plasmas **1**, 1403 (1994).
11. Surko, C. M. and Murphy, T. J., Phys. Fluids **B2**, 1372 (1990); Greaves, R. G., Tinkle, M. D. and Surko, C. M., Phys. Plasmas **1**, 1439 (1994).
12. Davidson, R. C., "Physics of Nonneutral Plasmas" (Addison-Wesley, Redwood City, California 1990).
13. Brown, L. S. and Gabrielse, G., Rev. Mod. Phys. **58**, 233 (1986).
14. Malmberg, J. H. and de Grassie, J. S., Phys. Rev. Lett. **35**, 577 (1975).
15. Davidson, R. C., J. Plasma Phys. **6**, 229 (1971).
16. Davidson, R. C., "Physics of Nonneutral Plasmas" (Addison-Wesley, Redwood City, California 1990), p. 300.
17. Douglas, M. H. and O'Neil, T. M., Phys. Fluids **21**, 920 (1978).
18. Malmberg, J. H. and Driscoll, C. F., Phys. Rev. Lett. **44**, 654 (1980).
19. Driscoll, C. F. and Malmberg, J. H., Phys. Rev. Lett. **50**, 167 (1983).
20. Malmberg, J. H., O'Neil, T. M., Hyatt, A. W. and Driscoll, C. F., Proc. 1984 Sendai Symposium on Plasma Nonlinear Phenomena, 31 (1984).
21. O'Neil, T. M., Phys. Fluids **23**, 2216 (1980).
22. Davidson, R. C. and Krall, N. A., Phys. Fluids **13**, 1543 (1970).
23. Landau, L. D. and Lifshitz, E. M., "Statistical Physics" (Addison-Wesley, Reading, Massachusetts 1974), pp. 11, 99.
24. Prasad, S. A. and O'Neil, T. M., Phys. Fluids **22**, 278 (1979).
25. Krall, N. A. and Trivelpiece, A. W., "Principles of Plasma Physics" (McGraw-Hill, New York 1973), p. 349.
26. Turner, L., Phys. Fluids **30**, 3196 (1987); Jeffries, J. B., Barlow, S. E. and Dunn, G. H., Int. J. Mass Spectrom. Ion Processes **54**, 169 (1983).
27. Davidson, R. C., "Physics of Nonneutral Plasmas" (Addison-Wesley, Redwood City, California 1990), p. 41.
28. Malmberg, J. H. and O'Neil, T. M., Phys. Rev. Lett. **39**, 1333 (1977).
29. Ichimaru, S., Rev. Mod. Phys. **54**, 1017 (1982).
30. Dubin, D. H. E., Phys. Rev. **A42**, 4972 (1990).
31. Dubin, D. H. E. and O'Neil, T. M., Phys. Rev. Lett. **60**, 511 (1988).
32. Rahman, A. and Schiffer, J., Phys. Rev. Lett. **57**, 1133 (1986).
33. Totsuji, H., in "Strongly Coupled Plasma Physics," (Edited by F. Rogers and H. DeWitt) (Plenum, New York 1987), p. 19.
34. Hasse, R. and Avilov, V., Phys. Rev. **A44**, 4506 (1991).
35. Tsuruta, K. and Ichimaru, S., Phys. Rev. **A48**, 1339 (1993).
36. Landau, L. D. and Lifshitz, E. M., "Statistical Physics" (Addison-Wesley, Reading, Massachusetts 1974), p. 53.
37. Metropolis, N., Rosenbluth, A. W., Rosenbluth, M. N. and Teller, E., J. Chem. Phys. **21**, 1087 (1953).
38. Dubin, D. H. E., Phys. Rev. **A40**, 1140 (1989).
39. Schiffer, J., personal communication.

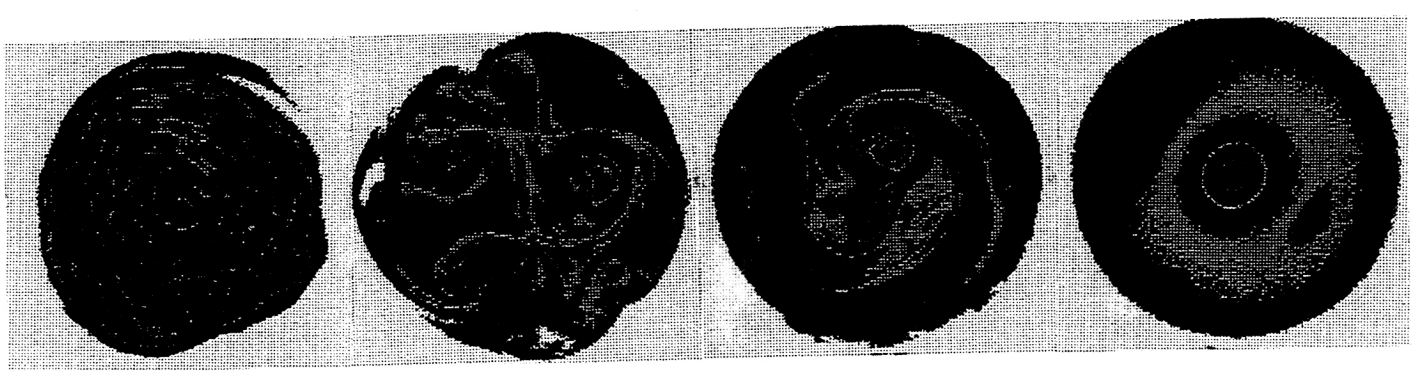

Fig. 20. Turbulent evolution from an unstable initial state.

40. Dubin, D. H. E., Phys. Rev. Lett. **66**, 2076 (1991).
41. Dubin, D. H. E., Phys. Fluids **B5**, 295 (1993).
42. Heinzen, D. J., Bollinger, J. J., Moore, F. J., Itano, W. M. and Wineland, D. J., Phys. Rev. Lett. **66**, 2080 (1991).
43. Bollinger *et al.*, Phys. Rev. **A48**, 525 (1993).
44. O'Neil, T. M. and Hjorth, P. G., Phys. Fluids **28**, 3241 (1985); Glinsky, M. E., O'Neil, T. M., Rosenbluth, M. N., Tsuruta, K. and Ichimaru, S., Phys. Fluids **B4**, 1156 (1992).
45. Beck, B. R., Fajans, J. and Malmberg, J. H., Phys. Rev. Lett. **68**, 317 (1992); Malmberg, J. H., Plasma Physics and Controlled Fusion **34**, 1767 (1992).
46. Chen, S. J. and Dubin, D. H. E., Bull. Am. Phys. Soc. **37**, 1415 (1992).
47. Fine, K. S., Driscoll, C. F., Malmberg, J. H. and Mitchell, T. B., Phys. Rev. Lett. **67**, 588 (1991).
48. Moore, D. W. and Saffman, P. G., J. Fluid Mech. **69**, 465 (1975); Saffman, P. G. and Szeto, R., Phys. Fluids **23**, 2339 (1980).
49. Rossow, V. J., J. Airer. **14**, 283 (1977).
50. Melander, M. V., Zabusky, N. J. and McWilliams, J. C., J. Fluid Mech. **195**, 303 (1988).
51. Driscoll, C. F. *et al.*, "Vortices, Holes, and Turbulent Relaxation in Sheared Electron Columns," to appear in Proc. 15th intl. Conf. Plasma Physics and Controlled Nuclear Fusion Research (Madrid, Spain 1994).
52. Huang, X.-P. and Driscoll, C. F., Phys. Rev. Lett. **72**, 2187 (1994).